



Article

Segregation of Fast-Reactive Species in Atmospheric Turbulent Flow

Guy P. Brasseur ^{1,2,3,*}, Mary Barth ¹, Jan Kazil ^{4,5} , Edward G. Patton ¹ and Yuting Wang ³ 

¹ National Center for Atmospheric Research, Boulder, CO 80307, USA; barthm@ucar.edu (M.B.); patton@ucar.edu (E.G.P.)

² Max Planck Institute for Meteorology, 20146 Hamburg, Germany

³ Department of Civil and Environmental Engineering, The Hong Kong Polytechnic University, Hung Hom, Kowloon, Hong Kong 999077, China; yuting.wang@polyu.edu.hk

⁴ Cooperative Institute for Research in Environmental Sciences, University of Colorado, Boulder, CO 80309, USA; jan.kazil@noaa.gov

⁵ National Oceanic and Atmospheric Administration, Chemical Sciences Laboratory, Boulder, CO 80305, USA

* Correspondence: brasseur@ucar.edu or guy.brasseur@mpimet.mpg.de

Abstract: Atmospheric turbulence, which produces chaotic motions in the planetary boundary layer, can inhibit mixing between fast-reacting species produced or released at different locations. This segregation process modifies the effective rate at which reactions occur between these species and is not appropriately accounted for in coarse-resolution models, since these models assume complete mixing of tracers within each grid box. Here, we present a few examples of large-eddy simulations (LES) applied to chemically reactive species in a forested area with high emissions of biogenic hydrocarbons, an urban area rich in anthropogenic emissions, and a maritime area with high emissions of reduced sulfur species.

Keywords: turbulence; chemistry; segregation; LES



Citation: Brasseur, G.P.; Barth, M.; Kazil, J.; Patton, E.G.; Wang, Y. Segregation of Fast-Reactive Species in Atmospheric Turbulent Flow. *Atmosphere* **2023**, *14*, 1136. <https://doi.org/10.3390/atmos14071136>

Academic Editors: Boris Galperin, Annick Pouquet and Peter Sullivan

Received: 10 May 2023

Revised: 6 July 2023

Accepted: 8 July 2023

Published: 11 July 2023



Copyright: © 2023 by the authors. Licensee MDPI, Basel, Switzerland. This article is an open access article distributed under the terms and conditions of the Creative Commons Attribution (CC BY) license (<https://creativecommons.org/licenses/by/4.0/>).

1. Introduction

The simulation of chemically reacting systems in turbulent flows has received considerable attention in recent years. The first applications focused on combustion processes and have allowed for progress, for example, in the design of a large number of industrial systems. At the same time, models with an explicit representation of turbulence in the atmosphere have been used to investigate the dispersion and fate of air pollutants. For example, Herring and Wyngaard [1] examined the behavior of a tracer undergoing a first-order decay in a convective flow and, using a detailed simulation, showed that the eddy diffusion applied to species concentrations must be represented by a nonlocal diffusion operator. Advances in computational fluid dynamics (CFD) techniques and the development of detailed chemical mechanisms have allowed for accurate air pollution simulations for the atmospheric boundary layer, especially in regions with inhomogeneous surface emissions. Furthermore, flux measurements obtained from surface or airborne instrumentation using eddy covariance techniques have provided experimental information on surface emissions and on convective exchanges in the lowest layers of the atmosphere.

In many applications, the spatial distribution and temporal evolution of chemical species in the atmosphere are derived by relatively coarse mathematical models that take into account emissions of primary constituents, in situ transformations, multiscale transport processes, and surface deposition. Models that describe these processes at a global or regional scale are constrained by the spatial resolution adopted to solve the model equations and by the resolution at which driving quantities such as surface emissions are provided. In such models, the reactive species are assumed to be entirely mixed within each grid box, and the likely subgrid segregation between these species is therefore ignored.

Such segregation, which is most prominent for constituents that chemically transform at similar time scales as the air motions, results from the small-scale inhomogeneities in the emissions and the complex nature of the turbulent flow. Figure 1 demonstrates how boundary-layer turbulence organizes itself differently under shear vs. buoyancy influences [2].

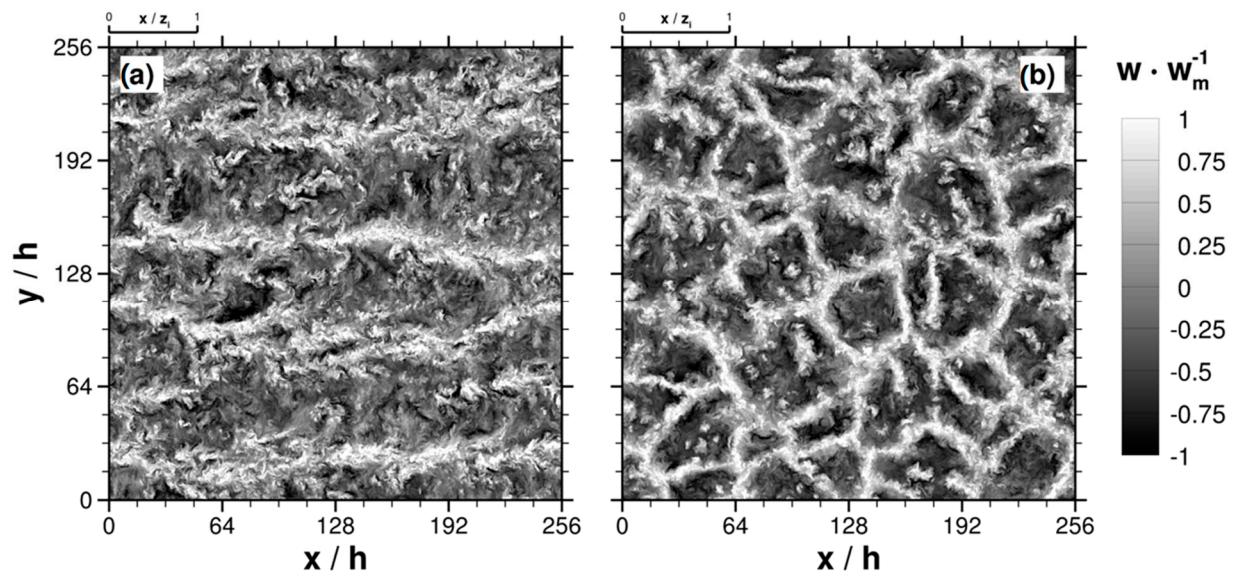


Figure 1. Instantaneous horizontal slices of vertical velocity (normalized by a characteristic velocity scale (w_m)) at a height of 120 m ($z/h = 6$) above a 20 m tall forest (h) from two turbulence-resolving atmospheric boundary layer simulations of differing stabilities. The left panel (a) is from an atmospheric boundary layer simulation with near-neutral stability, where the vertical shear of horizontal wind speed dominates the turbulence ($z_i/L \sim -1$; z_i is the depth of the atmospheric boundary layer, and L is the Monin–Obukhov length), and the right panel (b) is from a similar simulation but where buoyancy dominates the turbulence ($z_i/L \sim -\infty$) (see Patton et al. [2] for additional details). Of importance for turbulence–chemistry interactions is (1) that the character of organization in the turbulence transitions from elongated roll-like structures in shear-dominated near-neutral conditions to a cellular hexagon-like structure under buoyantly dominated conditions and (2) that surface-emitted species are most likely found within the narrow upwelling motions depicted in white, while species entrained from above the boundary layer are found primarily in the more broad, darker-colored regions. Figure adapted from Patton et al. [2] with the permission of © American Meteorological Society.

The mathematical concept of segregation can be introduced by first expressing the concentration $[A]$ of a chemical species (A) as the sum of its averaged value and the deviation relative to this average. Following the Reynolds decomposition formulation, we write $[A] = \overline{[A]} + [A']$, where the overbar refers to the average values, and the prime sign refers to the deviation from this average. If two species (A and B) react with each other, the corresponding reaction rate is expressed as

$$\frac{d[A]}{dt} = \frac{d[B]}{dt} = -k[A][B],$$

where k represents the rate constant of the reaction (assumed here to be a constant). The time evolution of the mean concentrations of A and B becomes

$$\frac{d\overline{[A]}}{dt} = \frac{d\overline{[B]}}{dt} = -k \left\{ \left(\overline{[A]} \cdot \overline{[B]} \right) + \overline{[A'] [B']} \right\} = -k \left(\overline{[A]} \cdot \overline{[B]} \right) (1 + I_{AB}),$$

where

$$I_{AB} = \frac{\{ \overline{[A'] [B']} \}}{(\overline{[A]} \cdot \overline{[B]})}$$

represents the segregation intensity [3], which is proportional to the covariance of the two reactants' concentrations. If chemical species A and B are entirely mixed, the segregation intensity is equal to zero, and the Damköhler number (D_a) [4], defined as the ratio between the turbulence time scale τ_{turb} and the chemical timescale (τ_{chem}),

$$D_a = \frac{\tau_{\text{turb}}}{\tau_{\text{chem}}}$$

is smaller than 1. If, however, the chemical lifetime of the two species is small, with a Damköhler number larger than one, the segregation intensity is negative and varies between 0 and -1 . In this case, for species whose emissions are not colocated, the reaction rate is considerably lower than if the two species were perfectly mixed. A value of -1 refers to fully segregated species with no reactions occurring between them. Reactants can also have positive covariance, thereby having an increased effective reaction rate compared to the well-mixed condition and a Damköhler number larger than 1. Mousavi et al. [5] showed that, in coarse models, this number can reach values close to 50, especially in the vicinity of pollution point sources, and recommended that irregular or adaptive grids be used to improve the simulation in the vicinity of these sources.

Chemical segregation in the lower layers of the atmosphere is affected by the structure and the strength of the flow, specifically by the boundary layer stability; the length scales of turbulence; the size of shear-driven and thermal structures; and, more generally, by the organization of turbulence in the dry and cloudy boundary layers. In numerical models, efficient mixing and tracer dispersion, which tends to be reduced by segregation, are therefore favored by high Reynolds numbers, high turbulence intensity, and high subscale diffusivity. Segregation is also influenced by the flow velocity and by buoyancy effects. The spatial and temporal distributions of surface emissions of reactive species impact how these species disperse and segregate.

Atmospheric chemistry is controlled by oxidation reactions between constituents that are emitted near the surface and oxidants that are not directly emitted from the surface but rather produced by photochemistry. It is more likely that segregation occurs between atmospheric reactants near strong source regions and an oxidant with higher mixing ratios above the boundary layer. An example of this scenario is the reaction between nitric oxide (NO) and ozone (O_3), where NO is emitted from combustion sources (anthropogenic and natural) and naturally from soils. Because ozone is produced through photochemistry in the atmosphere and deposited on the Earth's surface, its mixing ratios often increase with height above the surface. Other examples include reactions between volatile organic compounds (VOCs) and the hydroxyl radical (OH). The turbulence timescale varies diurnally and seasonally and can be different over land compared to oceanic regions. Typically, in the summer, the mid-day convective boundary layer over land (τ_{turb}) is 15 min, which means that chemical constituents with a lifetime of about 15 min may become segregated from their oxidants.

The effect of segregation on the mean atmospheric production or destruction of chemical species can be expressed in a coarse model by correcting the value of the original rate constants (k_{AB}). Using the Krol et al. [6] chemistry mechanism, Vinuesa and Vila-Guerau de Arellano [7] introduced the concept of an effective reaction rate (k_{AB}^{eff}) to parameterize the effect of segregation on chemical reactivity in coarse models. They wrote:

$$k_{AB}^{\text{eff}} = k_{AB}(1 + I_{AB})$$

In practice, such a correction is difficult to implement, since the value of the segregation intensity is constantly changing with the state of the turbulent flow. In fact, their approach

has not been tested with complex chemical mechanisms or in regional or global-scale chemistry transport models.

The covariance between the concentration of different species and, hence, the segregation coefficient can be derived from conventional Reynolds-averaged Navier–Stokes (RANS)-based simulations with an appropriate closure of the higher-order equations that involve the interactions between various turbulent fluctuations. Such an approach may be inaccurate if the averaged chemical reaction rates affected by the strong nonlinearity associated with the chemical mechanism are calculated on the basis of averaged parameters only. Although more computationally expensive than a RANS models, large-eddy simulation (LES) models spatially filter the equations of motion at sufficiently small scales compared to RANS that the largest energy-containing scales of the turbulence, which extracts energy from the mean flow, are resolved. In this case, only the smallest and nearly isotropic eddies that act primarily to dissipate energy are parameterized through a subgrid scale model [8–11]. In other words, RANS models completely parameterize the influence of turbulence, while LES models resolve the dominant turbulent motions.

Investigations in the atmospheric boundary layer using LES to study turbulence–chemistry interactions began with generic species A and B, where one species was emitted at the surface and the other entrained into the boundary layer from the free troposphere [12,13]. This simple configuration was necessitated by computational constraints in the 1990s. As computational capacity increased, studies emerged examining chemical systems of reactions, albeit using a simple representation [6].

In this paper written in honor of Jack Herring’s lifelong scientific accomplishments, we present a few examples of LES-based simulations applied to chemically reactive species in the atmospheric boundary layer under different environments: (1) in a forested area with high emissions of biogenic hydrocarbons, (2) in an urban area rich in anthropogenic emissions, and (3) over a maritime area with high emissions of reduced sulfur species.

2. Boundary Layer over a Forest

Forested land covers ~30% of Earth’s land surface [14]. Trees are strong emitters of volatile organic compounds (VOCs), especially isoprene emitted from broadleaf deciduous trees and terpenes from needleleaf trees. The emissions of these biogenic VOCs comprise 80% of the total global VOC emissions [15]. Isoprene and monoterpenes participate in atmospheric photochemistry, contributing to the production of ozone [16,17] and secondary organic aerosol (SOA; e.g., [18–21]). Thus, the emissions and chemistry of isoprene and monoterpenes are important sources and sinks to represent in chemistry transport models. For example, during daytime, isoprene emissions increase, depending on the temperature and amount of photosynthetic active radiation (PAR) reaching the vegetation. Isoprene readily reacts with hydroxyl radicals (OHs) to form peroxy radicals. The rate of the reaction between isoprene and OH is fast, so isoprene has a lifetime of 15–30 min, which is comparable to the turbulence turnover time of the atmospheric boundary layer (ABL).

Several studies have investigated the interactions between turbulence and chemistry over forested regions without considering the effects of the forest canopy on turbulent motions. Krol et al. [6] were the first to use a simple atmospheric chemistry mechanism (7 predicted trace gases using 10 photochemical reactions) to address segregation effects between reactants. Their simulations revealed that a highly reactive VOC with an ~18 min chemical lifetime (like that of isoprene) had an ABL average intensity of segregation of 20% for a domain with homogeneous emissions. Krol et al. [6] also examined the impact of heterogeneous emissions and found segregation to be even stronger for the VOC + OH reaction compared to the case with homogeneous emissions.

The segregation of isoprene and OH was suggested as a possible cause for large OH observations that could not be explained with known sources/sinks in the tropics [22,23]. To determine if this was a viable explanation, Ouwersloot et al. [24] performed LES simulations with 18 reacting trace gases and 19 chemical reactions and found that the segregation effect alone was not sufficient to reconcile modeled and observed OH concentrations. They

also showed that heterogeneous emissions enhance segregation of reactants (Figure 2) in accordance with Krol et al. [6] and Kaser et al. [25]. By obtaining high-temporal-resolution measurements of isoprene and OH just above a mixed deciduous forest near Julich, Germany, analyses of the 2003 Emission and CHemical transformation of biogenic volatile Organic compounds (ECHO 2003, [26]) case study produced estimates from measurements of the intensity of segregation between isoprene and OH for the 25 July 2003 case study [27,28]. Dlugi et al. [27] calculated 9–15% segregation between isoprene and OH during mid-day (1200–1300 CET) and <10% segregation for other analysis calculations between 1000 and 1400 CET. Dlugi et al. [28] extended the analysis of isoprene and OH segregation with the ECHO 2003 data, showing that both chemical transformations and dynamical processes (turbulent and convective mixing, as well as advection) are responsible for observed segregation. Kaser et al. [25] calculated a measurement-based budget of isoprene in the atmospheric boundary layer using aircraft data from the 2013 Southern Oxidant and Aerosol Study (SOAS). Combining measurement analysis, detailed chemistry box modeling, and large-eddy simulations to separate the roles of chemistry and heterogeneous emissions, Kaser et al. [25] found that the surface heterogeneity of isoprene emissions segregated isoprene and OH by up to 30%.

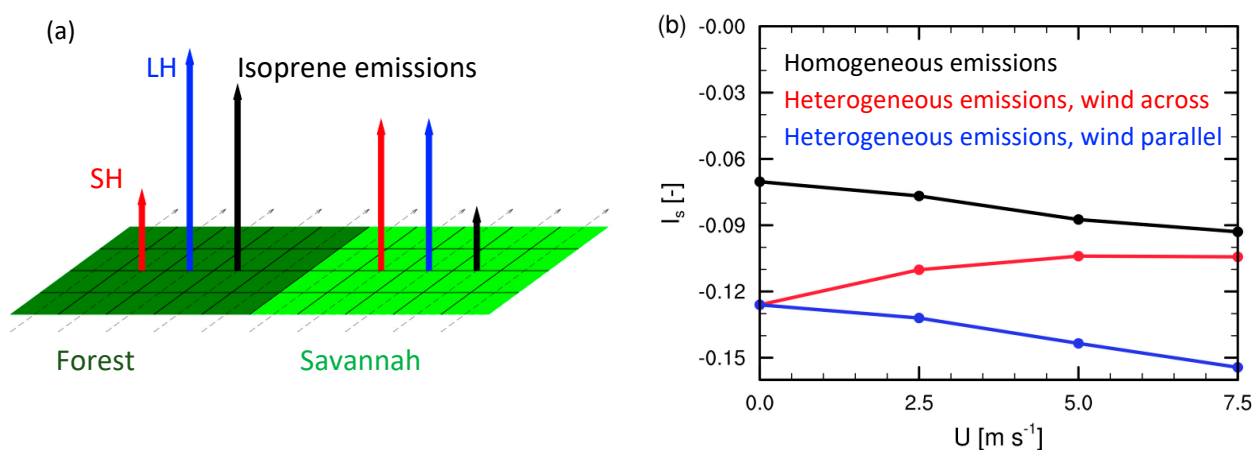


Figure 2. (a) Schematic of imposing heterogeneous emissions of sensible heat (red), latent heat (blue), and isoprene (black) surface emissions used by Ouwersloot et al. [24]. (b) Intensity of segregation for isoprene and OH in the ABL as a function of the horizontal wind for LES studies of homogeneous and heterogeneous emissions. In (b), the blue line corresponds to wind blowing parallel between the forest and savannah patches, while the red line corresponds to wind blowing across from forest to savannah. Figure adapted from Ouwersloot et al. [24], © Author(s) 2011, licensed under a Creative Commons Attribution (CC BY) 3.0 License.

Many of these early LES applications of ABL chemistry used simple chemical mechanisms, leaving questions as to whether more complex chemistry reduces the effect of segregation through its role in producing OH from other reactions. As computational capabilities increased, additional studies were pursued utilizing LES models that included atmospheric chemistry reaction schemes of varying complexity. These studies investigated the impact of fair-weather cumulus clouds [29–31], the role of varying nitrogen oxide ($\text{NO}_x = \text{NO} + \text{NO}_2$) scenarios (from very low NO_x found in remote regions to very high NO_x found in urban forest centers [32]), and the effect of varying weather scenarios [33]. These studies found that the presence of fair-weather cumulus clouds causes venting of the ABL, increasing the segregation between the surface-sourced isoprene and in situ-formed OH reactants in the cloud layer [29]. Kim et al. [30] applied LES coupled with a more complex chemistry scheme (52 reacting trace gases and 142 reactions) to summertime, fair-weather cumulus convective ABL. They found that the combined effect of modified photodissociation rates and isoprene emissions via cloud shading due to cloud scattering of solar radiation did not impact isoprene and OH radical mixing ratios substantially [30],

as the two effects tended to offset each other. However, the dissolution of soluble trace gases and subsequent aqueous-phase chemistry within the cloud droplets enhanced the segregation between reactants [31] within the cloud layer (Figure 3). Kim et al. [32] showed that the covariance of isoprene and OH in the mixed layer ($z = 500$ m) depended on NO_x levels, with the largest segregation of 18% occurring for $\text{NO}_x = 8\text{--}10$ ppbv, the smallest segregation of 5% for $\text{NO}_x = 1\text{--}2$ ppbv, and $\sim 6\%$ segregation for $\text{NO}_x = 0.1\text{--}0.3$ ppbv. By conducting LES with chemistry runs for three case studies of the DISCOVER-AQ field campaign, Li et al. [33] found that segregation between isoprene and OH was larger (10% segregation) for a hot, humid day than for a clear-sky, cool summer day scenario and a moderately warm day with fair-weather cumulus clouds. Under hot, humid, and convective conditions, the isoprene and oxygenated VOC lifetimes lengthened due to higher isoprene emissions, elevated initial chemical concentrations, and competition among VOCs for reaction with OH.

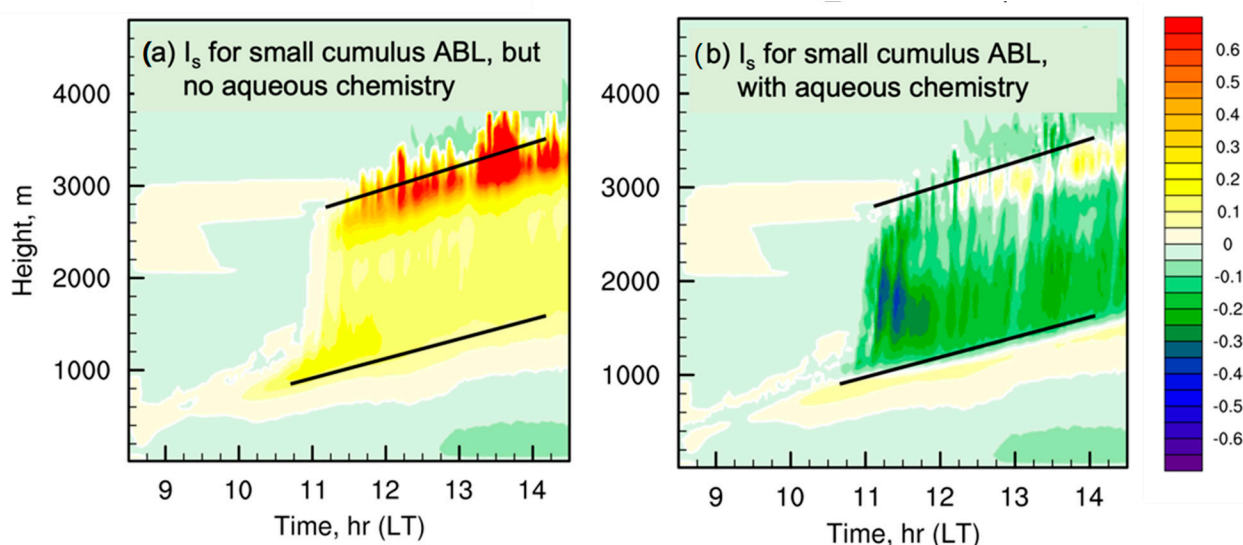


Figure 3. Temporal evolution of the horizontally averaged intensity of segregation for isoprene and OH from the NCAR LES using (a) relatively complex gas-phase chemistry only and (b) gas-phase and aqueous-phase chemistry. The black lines in panels (a,b) roughly mark the cloud base and cloud top of the cloudy layer. The cloud top and base are defined as the maximum and minimum heights where liquid water is present in the model domain, respectively. The figure is based on that from Li et al. [31], with the permission of © WILEY.

By absorbing momentum throughout its distributed depth, tall trees alter ABL turbulent motions by creating a hydrodynamically unstable inflection point in the mean vertical wind profile. Large ABL-scale turbulent motions trigger instability when bringing high-momentum fluid down to the canopy top, thereby enhancing the vertical shear of the horizontal wind, which produces pairs of head-up and head-down vortices whose scales are thought to be set by the vorticity thickness at the canopy top [34,35]. These canopy-induced turbulent motions are thought to perform 60–80% of the exchange between the canopy layers and aloft and can be regularly identified in tower-based field data as sweep (downwelling) and ejection (upwelling) motions separated by a scalar microfront [36,37]. In weak-wind, buoyantly dominated conditions, buoyant plumes from the ground and canopy drive the exchange between the canopy layers and aloft [2,38,39].

Organized turbulent motions therefore transport trace gases from the canopy into the ABL, which affects the above-canopy tropospheric chemistry. Trace gases are also transported into the forest canopy, where within-canopy photochemistry and dry deposition can remove important trace gases. Within the canopy, organized turbulent structures lead to spatial variability of reactants, resulting in segregations of reactants. Clifton et al. [40] used an LES coupled to a multilayer canopy model with a simple chemical mechanism (19 trace

gases with 41 reactions) to examine the interactions between the canopy, turbulence, and atmospheric chemistry. Their results for specific cases showed that segregation within the canopy altered reaction rates substantially (from 48% segregation to 23% positive covariance). They illustrated that high soil NO emissions promote more segregation among reactants and that high horizontal spatial variability of reactants within the forest canopy plays a role in separating reactants, as previously shown by Krol et al. [6], Dlugi et al. [28], Kaser et al. [25], and Patton et al. [2].

These previous LES studies either employed simple atmospheric chemistry schemes with highly detailed turbulence representation or reduced the resolution of the LES to include more complex chemistry. There is a strong need to represent both turbulence and chemistry in detail (i.e., high-resolution LES with complex chemistry mechanisms) and represent in-canopy and above-canopy gas-phase and aerosol chemistry. The role of aerosols in affecting heating rates, surface-sensible and latent heat fluxes, and ABL structure has been examined for idealized convective boundary-layer regimes [41,42]. The impact of aerosols on the ABL needs to be extended to learn about the subsequent impact on chemical reactivity. Aerosol impacts on ABL composition and chemical reactivity should be investigated further through combined field experiments and modeling analysis, as aerosols are complex in terms of their spatial variability, optical properties, and composition. To evaluate and gain further insight into the processes affecting chemical composition in the ABL, field observations with strategically placed towers and aircraft measurements must be pursued.

3. Urban Boundary Layer

Segregation effects are significant when (1) the reaction rate is fast [43], (2) the emission sources of the reacting species are spatially inhomogeneous [24,44], or (3) the emissions of one chemical compound are intense [32,45]. In urban areas, the emissions produced by human activities are usually characterized by heterogeneous distributions. An example is provided by the traffic emissions taking place on different roads. Furthermore, in polluted cities, anthropogenic emissions are intense, especially road traffic emissions, while industrial facilities and power plants produce additional pollution. Therefore, the segregation effect is an important factor for understanding air pollution in large cities.

Atmospheric chemistry in urban areas involves OH oxidation of anthropogenic VOCs and biogenic VOCs (similar to the processes discussed for the forested boundary layer) and their chemistry with NO and NO₂, which produces O₃. The segregation effect of fast-reacting chemical reactants in the turbulent urban environment with spatially heterogeneous emissions needs to be addressed. In some previous studies, a simple NO–NO₂–O₃ mechanism (with three reactions) was coupled with microscale models because of the potential for NO, which is emitted from anthropogenic surface sources, and O₃ to be segregated. For instance, Baker et al. [46] introduced O₃–NO_x chemistry into a CFD-LES model and applied it in an idealized street canyon. They showed that the variations in the chemical species were largely affected by the turbulent structures at the different locations of the canyon. Auger and Legras [47] adopted a more comprehensive chemical mechanism with 44 species in an LES model for urban application and pointed out that the segregation effect was strong if the emissions were restricted to a limited area, especially during the morning, when mixing is incomplete. Bright et al. [48] compared their CFD-LES model with coupled chemistry to a zero-dimensional box model to investigate the impact of segregation in street canyons. Their LES simulation resulted in lower NO_x (−3%), OH (−11%), and HO₂ (−8%) concentrations but higher O₃ (6%) values relative to the results of a box model for their designed scenario. Zhong et al. [49,50] compared the segregation effect between deep and regular urban street canyons, which is dependent on the aspect ratio, and revealed that this effect was greater in deeper street canyons due to the vertically aligned vortex structures present in the poorly mixed environment.

Li et al. [44] conducted a more systematic analysis of the segregation effect under urban-like conditions through a series of DNS experiments. A simple second-order $A + B \rightarrow C$

reaction was adopted, and the effects on the segregation intensity resulting from the reaction rate, the strength of the emission fluxes, and the heterogeneity in the emissions were calculated. Their study showed that the segregation intensity increased considerably when the surface emissions of one chemical compound was enhanced from rural to urban values because the availability of the other tracer became limited. Spatial heterogeneity also has an important impact on the segregation intensity.

The above studies were performed either by CFD models in an idealized street block or by LES/DNS models in a flat domain. Wang et al. [51] developed an LES experiment based on a realistic case in the vicinity of Hong Kong Island with complex topography, land use, and emission distributions (Figure 4a,b). A simplified O_3 photochemical mechanism was adopted with 15 species and 18 reactions. As Hong Kong Island is characterized by a special landscape with large forest areas in the mountainous region in the island's center and a dense built-up urban canopy along the coast, both anthropogenic and biogenic emission sources are important, although geographically separated. This work discussed the factors that affect segregation in a polluted situation. The results showed that heterogeneity in emissions is the dominant factor that causes large segregation in the urban area. Topography has an influence on the turbulent structure and can therefore affect segregation locally. The segregation intensity for the reaction of $NO + O_3 \rightarrow NO_2$ can reach about -40% in the urban area, especially on the leeward slope of the mountains (Figure 4c,d).

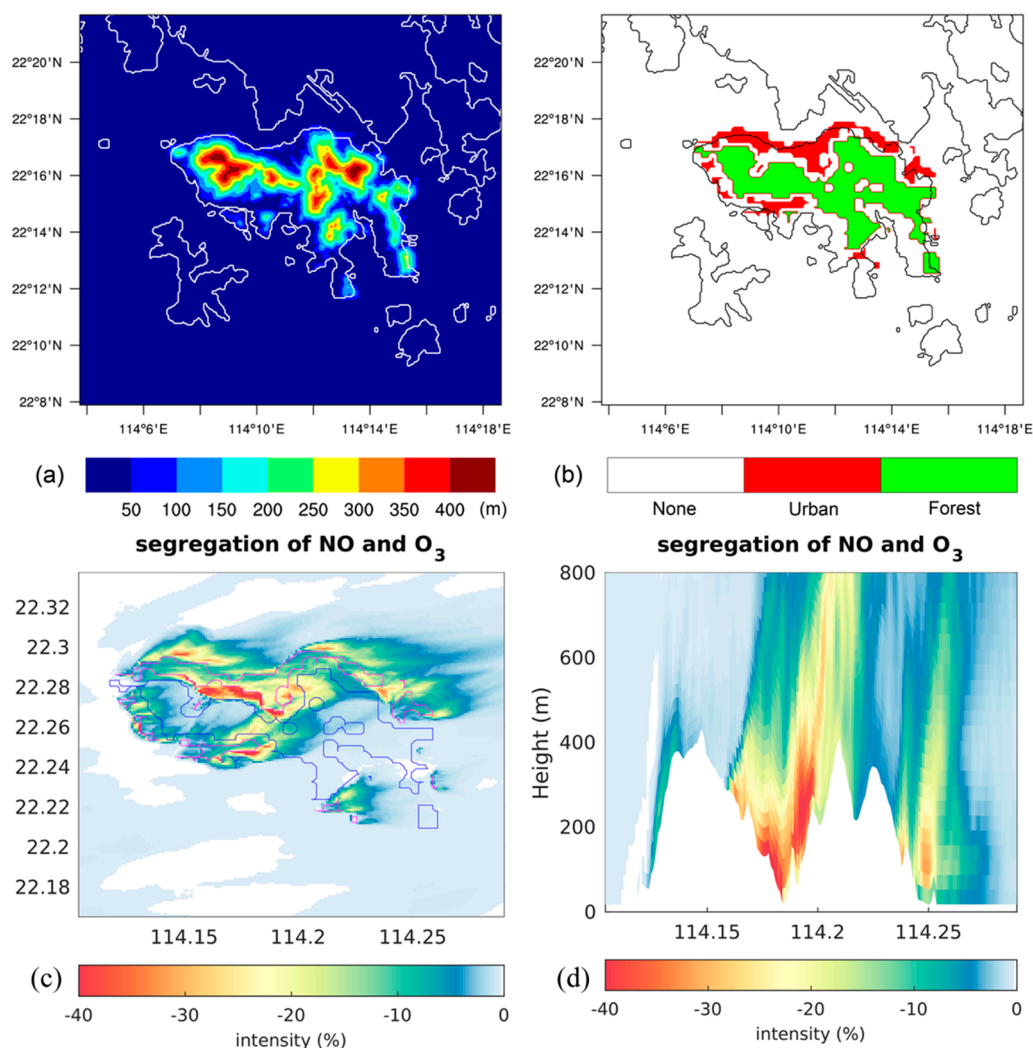


Figure 4. (a) Terrain height of Hong Kong Island; (b) emissions map adopted based on the land use (red: anthropogenic emissions from urban areas; green: biogenic emissions from forested areas); (c) segregation intensity near the surface (the magenta line shows the urban area, and the blue line shows

the forested area); (d) vertical cross section along latitude 22.275° N. Figure adapted from Wang et al. [51] as an illustration of the idealized LES modeling for a convective PBL over a polluted urban environment. This study adopted two nested domains with the outer domain ($\Delta x = 300$ m) to provide the initial and boundary conditions for the inner domain ($\Delta x = 100$ m), as shown in the figure. The experiment was initialized from the output of the mesoscale WRF ($\Delta x = 1$ km), and the prevailing wind is westerly. © Author(s) 2021, licensed under a Creative Commons Attribution (CC BY) 4.0 License.

In a subsequent study, Wang et al. [52] set up several control runs with different strengths of emission fluxes to account for clean and less polluted conditions (the anthropogenic emission rates were reduced by two orders of magnitude for NO, CO, and VOCs). Their study shows that the pollution levels have an important impact on the distributions of O_3 and OH oxidants due to their reactions with the primary pollutants. The segregation intensities between the anthropogenic VOCs and OH radicals are also largely influenced by the pollution level, while the biogenic VOCs are less affected.

Some recent studies reported realistic simulations of chemical species using coupled meso-to-microscale models. For instance, Wang et al. [53] performed multiscale simulations with coupled WRF-LES-Chem for Hong Kong with the highest spatial resolution of 33 m. Figure 5a,b show the near-surface noontime distribution of NO and O_3 in the innermost domain covering the Kowloon peninsula and the northern coast of Hong Kong Island. Figure 5c highlights the calculated segregation between NO and O_3 . High segregation intensity is found near the location of road traffic emissions and on the leeward slope of the mountain, which is consistent with the idealized experiment discussed above.

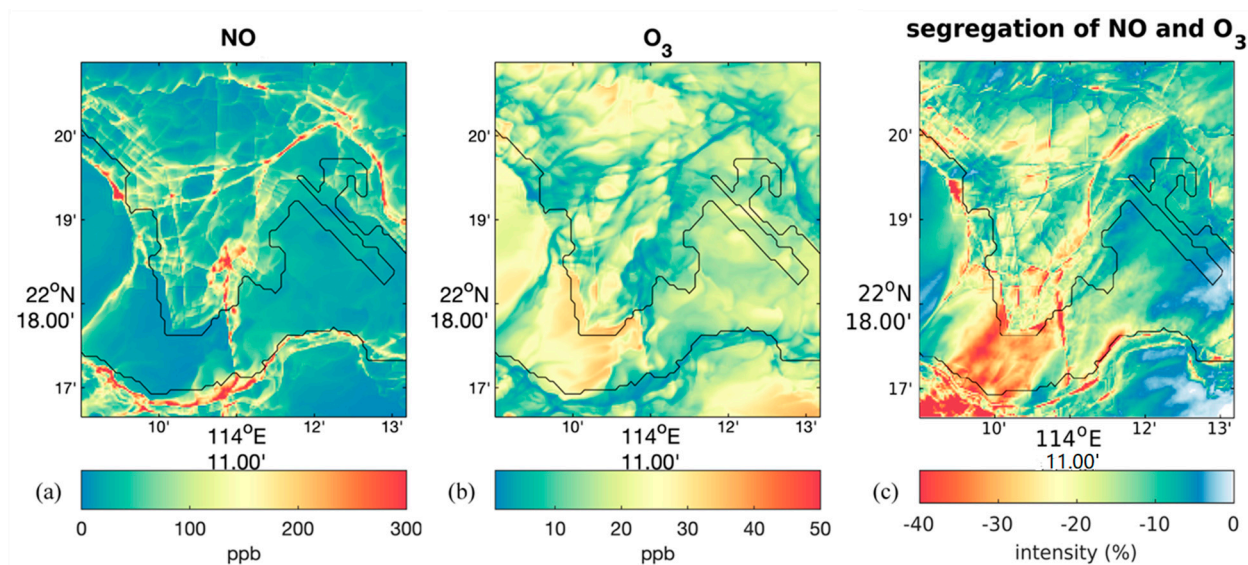


Figure 5. The distribution of NO (a) and O_3 (b) near the surface at noontime adapted from the 33 m WRF-LES-Chem simulation by Wang et al. [53], © Author(s) 2023, licensed under a Creative Commons Attribution (CC BY) 4.0 License. and the segregation intensities between NO and O_3 (c) calculated from the concentrations of NO and O_3 shown in this figure.

4. Clouds, Turbulence, and Biogenic Sulfur in the Marine Boundary Layer

The marine boundary layer (MBL) extends from the ocean surface to a capping inversion that separates it from the free troposphere. Ocean-emitted chemical species are transformed in the MBL by radiation, as well as gas- and aqueous-phase chemistry, and by aerosol and cloud processes. Gas-phase conversion is commonly started by reactions with short-lived, photochemically produced reactants, such as the hydroxyl radical (OH), which forms from ozone that is entrained into the MBL from the free troposphere. Thus,

biogenic sulfur compounds emitted from the oceans, primarily dimethyl sulfide (CH_3SCH_3 , DMS), hydrogen sulfide (H_2S), carbonyl sulfide (OCS), and carbon disulfide (CS_2), are oxidized to sulfur dioxide (SO_2), sulfuric acid (H_2SO_4), methanesulfonic acid ($\text{CH}_3\text{SO}_3\text{H}$), hydroperoxymethyl thioformate ($\text{HOOCH}_2\text{SCHO}$, HPMTF [54]), and ultimately sulfate (SO_4^{2-}). This alters the aerosol population by nucleation of new particles in the gas phase and by growth through gas-phase condensation and aqueous-phase mass accumulation. Condensation of water vapor may turn aerosol particles into cloud droplets. This connects biogenic sulfur emissions from the oceans to MBL clouds, which are sensitive to aerosol and exert leverage over the Earth's radiation budget [55].

Chemical segregation is determined by MBL dynamics, which are driven by surface-sensible and latent heat fluxes, by radiative heating and cooling, and by wind shear. Decoupling, a common [56] phenomenon that stratifies the MBL into a lower layer above the ocean and an upper, cloud-free or cloudy layer below the inversion, contributes to segregation. Due to the strong radiative cooling at their tops and the process of latent heating and cooling, clouds reinforce MBL circulation, increase mixing, and counteract segregation. Thus, clouds play an important role in the segregation of chemical species in the MBL.

We explore how trade cumulus cloud organization and the associated mesoscale dynamics shape the distribution of an ocean-emitted species and modulate its segregation relative to a free-tropospheric species. Figure 6 shows snapshots taken on 2 February 2020 at 17 h 00 m 00 s UTC from an LES of the sugar-to-flower transition following Narenpitak et al. [57]. The simulation starts on 2 February 2020 at 00 h 00 m 00 s UTC and tracks two tracers with a lifetime of 24 h. One tracer is initialized with 0.6 ppt in the boundary layer and 0 ppt in the free troposphere and is emitted at $8.6 \mu\text{mol m}^{-2} \text{d}^{-1}$ from the ocean. The other tracer is initialized with 0 ppt in the boundary layer and 3 ppt in the free troposphere and has no surface source or sink.

The cloud field contains several “Flower” clouds [58] with stratiform outflows near their tops and cold pools at the surface surrounded by small cumuli (Figure 6a). Figure 6b shows the segregation intensity of the two tracers in the MBL. Segregation intensity is reduced at the locations of the Flower clouds relative to the surrounding areas with isolated trade cumulus clouds. The reduced segregation is caused by mesoscale circulation and vertical transport in the Flowers clouds. Figure 6c,d show the distribution of the surface-emitted tracer, and Figure 6e,f show the distribution of cloud water along two transects through the cloud field (Figure 6a). At the location of cumulus cluster “A”, an early stage of Flower clouds, circulation on the mesoscale that is associated with the formation of moist patches in which Flowers form [57] creates a tracer patch in the cumulus layer (Figure 6b). The tracer is lofted from the mixed layer by individual cumulus updrafts, some of which rise as high as 2600 m (Figure 6e). At the location of mature Flower cloud “B”, the aggregated cumulus updrafts forming the Flower loft large amounts of the tracer from the mixed layer upward (Figure 6d). The aggregated nature of the Flower is evident from the distribution of cloud water (Figure 6f). Additionally, smaller structures in the tracer distribution in the cloud layer shaped by the mesoscale circulation of the Flower cloud state appear along both transects (Figure 6c,d).

The tracer distribution in the Flower cloud state (Figure 6) is an idealized approximation of the distribution of a surface-emitted species such as DMS. In the case of DMS, a part is scavenged inside the cumulus clouds. The remainder undergoes rapid oxidation by OH near cloud tops due to enhanced actinic fluxes, possibly with a lifetime shorter than 24 h, to SO_2 , H_2SO_4 , and other sulfur species and potentially initiates aerosol nucleation. Despite the idealization, the example illustrates that trade cumulus clouds act as a valve for the transport of ocean-emitted species from the mixed layer into the boundary layer above. Trade cumulus cloud organization shapes the resulting distribution, with potential consequences for chemical conversion and new particle formation.

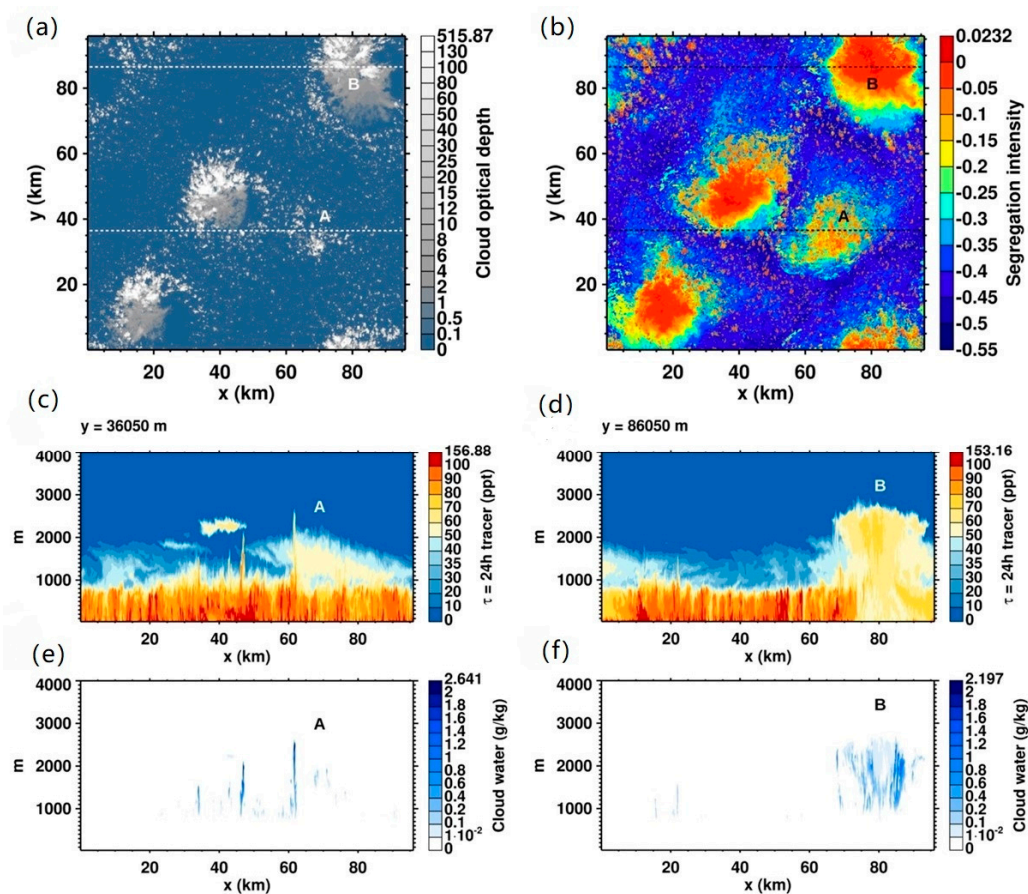


Figure 6. “Flower”-type trade cumulus organization in the Caribbean east of Barbados on 2 February 2020 at 13 h 00 m 00 s local solar time simulated by Narenpitak et al. [57]. (a) Cloud optical depth. (b) Segregation intensity of a surface-emitted tracer and a free-tropospheric tracer with lifetimes of $\tau = 24$ h. The mixing ratio of the surface-emitted tracer (c,d) and cloud water content (e,f) are shown along two transects. “A” denotes the location of a cumulus cluster, an early stage of “Flower” development, and “B” denotes the location of a mature “Flower” aggregate.

5. Outlook

Spatial segregation of reactants by organization in turbulence clearly participates the evolution of those reactants in the ABL. The importance of segregation in modulating reaction rates in the ABL varies with the scale of the separation distance of sources/sinks and with the chemical or atmospheric regime.

Due to the need to simultaneously sample multiple species at sufficiently fast time scales to interrogate the role of the organized structures comprising the turbulence (with time scales ranging from milliseconds to hours) in controlling reaction rates, species–species covariances (and, hence, segregation) have proven difficult to measure. As such, much of what the community currently knows about species–species segregation comes from idealized modeling.

To advance predictive skill, the community needs to surmount critical hurdles in observing and simulating turbulence–chemistry interactions. While instruments like PTR-ToF-MS (proton-transfer reaction time-of-flight mass spectrometry) enable rapid sampling across a range of chemical masses, they remain prohibitively expensive and are not conducive to sampling in regimes with condensed cloud water, which limits their utility due to the ubiquitous spatial heterogeneity of reactant sources/sinks in the ABL. When attempting to interrogate the spatial variation of species–species covariances, sampling with a single instrument requires substantial compromises. Sampling strategies need to be designed to measure both the turbulence and the chemistry. While profiles on a

single tower provide information on locally occurring near-surface processes controlling species–species segregation, reactions occurring near the surface can be strongly influenced by the diurnal evolution of the boundary layer as it grows and decays each day in response to solar forcing (through both dilution due to the larger volume into which species are mixed and entrainment of reacting species from aloft, e.g., [59,60]). While flying an instrument like a PTR-ToF-MS through the boundary layer on an aircraft can provide vertical profile information, flying sufficiently long horizontal legs to sample the full range of scales within the ABL turbulence ensures that only a limited number of heights can be sampled within a timeframe that one might be able to consider the turbulence and chemistry reasonably stationary. Therefore, the community would truly benefit from the development of remote (e.g., lidar) and in situ sensing capabilities with sufficient power to continuously sample highly range- and time-resolved reactant profiles in both cloudy and cloudless conditions toward understanding of the spatially and diurnally varying evolution of species–species segregation across varying climates and chemical regimes.

Although LES resolves the largest energy-containing scales of turbulence performing reactant transport in the ABL (and the role of those large-scale structures in modulating reactivity), the influence of scales smaller than the grid resolution must still be parameterized. At those small scales, current LES practice generally assumes that reactants are treated as if they are passive, nonreacting scalars (e.g., [24,61]). Hence, segregation and chemical modification of flux–gradient relationships (e.g., [62,63]) are ignored at these scales. This assumption is made primarily for simplicity's sake, since the community does not yet sufficiently understand the spectral decomposition of turbulence–chemistry interactions necessary for the development of a parameterization that only applies at a certain scale and smaller. While numerous chemically aware subgrid models for LES have been proposed in the combustion engineering literature (e.g., [64,65]), these subgrid models typically rely on a priori knowledge of the joint probability density distribution of the reactants of interest; in the atmospheric boundary layer, such joint PDFs vary with atmospheric stability, height, and the chemical regime. For near-surface applications, a key opportunity to advance chemically aware subgrid models for LES could lie in adapting what have become known as horizontal array turbulence study strategies (HATS, e.g., [66–70]) to reactants. The HATS strategy uses time-synchronized spatial arrays of fast instrumentation to explicitly filter planes of field data into large and small scales. If such arrays were complemented with an equal number of PTR-ToF-MS instruments, one could interrogate spatially filtered species–species covariances (i.e., the joint PDF of the small scales) toward the development of a chemically aware subgrid-scale model and its variation with Damköhler number and atmospheric stability. Similar strategies could be undertaken by filtering DNS simulation data, but the role of the largest scales of motion would be lost.

At coarser resolutions, where turbulence is not resolved (i.e., in regional air quality and climate models), techniques to parameterize the influence of segregation on reactivity have been proposed (e.g., [7,61]); however, these techniques have only been evaluated for highly reduced chemistry. Attempts to incorporate the SOMCRUS framework [61] into today's weather and climate models have proven difficult due to the need to solve so many additional equations for the species–species covariance. Pathways to reduce the computational requirements remain elusive because of the continually evolving variation of the processes that dominate turbulence–chemistry interactions through diurnal and seasonal time scales and a lack of turbulence–chemistry-focused observations spanning the full ABL depth.

Nevertheless, there are abundant opportunities to advance the understanding and representation of the turbulence–chemistry interactions that control reactivity in the atmospheric boundary layer and in turbulent cloudy environments. Success requires research spanning traditional disciplinary boundaries; Jack Herring was one of the unique individuals who recognized this need.

Author Contributions: All authors were directly involved in the conceptualization, methodology, and writing of this paper. All authors have read and agreed to the published version of the manuscript.

Funding: The National Center for Atmospheric Research is sponsored by the US National Science Foundation. This research was supported in part by NOAA cooperative agreement NA22OAR4320151. YW contribution to this work is supported by the Hong Kong Research Grants Council (grant no. T24-504/17-N).

Data Availability Statement: This paper reviews studies published in the scientific literature and does not make use of new research data.

Conflicts of Interest: The authors declare no conflict of interest.

References

- Herring, J.R.; Wyngaard, J.C. Convection with a first-order chemically reactive passive scalar. In Proceedings of the Fifth International Symposium on Turbulent Shear Flows, Cornell University, Ithaca, NY, USA, 7–9 August 1987; pp. 324–336.
- Patton, E.G.; Sullivan, P.P.; Shaw, R.H.; Finnigan, J.J.; Weil, J.C. Atmospheric stability influences on coupled boundary layer and canopy turbulence. *J. Atmos. Sci.* **2016**, *73*, 1621–1647. [\[CrossRef\]](#)
- Danckwerts, P.V. The definition and measurement of some characteristics of mixtures. *Appl. Sci. Res.* **1952**, *3*, 279–296. [\[CrossRef\]](#)
- Damköhler, G. Influence of turbulence on the velocity flames in gas mixtures. *Z. Elektrochem. Angew. Phys. Chem.* **1940**, *46*, 601–626. [\[CrossRef\]](#)
- Mousavi, M.; Soltanieh, M.; Badakhshan, A. Influence of turbulence and atmospheric chemistry on grid size with respect to location in modeling and simulation of photochemical smog formation and transport. *Environ. Model. Softw.* **1999**, *14*, 657–663. [\[CrossRef\]](#)
- Krol, M.C.; Molemaker, M.J.; de Arellano, J.V.G. Effects of turbulence and heterogeneous emissions on photochemically active species in the convective boundary layer. *J. Geophys. Res. Atmos.* **2000**, *105*, 6871–6884. [\[CrossRef\]](#)
- Vinuesa, J.-F.; Arellano, J.V.D. Fluxes and (co-)variances of reacting scalars in the convective boundary layer. *Tellus B Chem. Phys. Meteorol.* **2003**, *55*, 935–949. [\[CrossRef\]](#)
- Smagorinsky, J. General circulation experiments with the primitive equations: I. The basic experiment. *Mon. Weather Rev.* **1963**, *91*, 99–164. [\[CrossRef\]](#)
- Lilly, D.K. On the application of eddy viscosity concept in the inertial sub-range of turbulence. *NCAR Tech. Note* **1966**, *123*, 19. [\[CrossRef\]](#)
- Lilly, D.K. The representation of small-scale turbulence in numerical simulation experiments. *Proc. IBM Sci. Comput. Symp. Environ. Sci.* **1967**, *23*, 195–210. [\[CrossRef\]](#)
- Deardorff, J.W. A numerical study of three-dimensional turbulent channel flow at large Reynolds numbers. *J. Fluid Mech.* **1970**, *41*, 453–480. [\[CrossRef\]](#)
- Schumann, U. Large-eddy simulation of turbulent diffusion with chemical reactions in the convective boundary layer. *Atmos. Environ.* **1989**, *23*, 1713–1727. [\[CrossRef\]](#)
- Sykes, R.I.; Parker, S.F.; Henn, D.S.; Lewellen, W.S. Turbulent mixing with chemical reaction in the planetary boundary layer. *J. Appl. Meteorol. Climatol.* **1994**, *33*, 825–834. [\[CrossRef\]](#)
- FAO. *Global Forest Resources Assessment 2020: Main Report*; 978-92-5-132974-0; Food and Agriculture Organization of the United Nations: Rome, Italy, 2020; p. 184.
- Olivier, J.G.J.; Berdowski, J.J.M. Global Emissions Sources and Sinks. In *The Climate System*; Berdowski, J., Guicherit, R., Heij, B.J., Eds.; AA Balkema Publishers: Lisse, The Netherlands, 2001; pp. 33–77.
- Chameides, W.L.; Lindsay, R.W.; Richardson, J.; Kiang, C.S. The role of biogenic hydrocarbons in urban photochemical smog: Atlanta as a case study. *Science* **1988**, *241*, 1473–1475. [\[CrossRef\]](#) [\[PubMed\]](#)
- Trainer, M.; Williams, E.J.; Parrish, D.D.; Buhr, M.P.; Allwine, E.J.; Westberg, H.H.; Fehsenfeld, F.C.; Liu, S.C. Models and observations of the impact of natural hydrocarbons on rural ozone. *Nature* **1987**, *329*, 705–707. [\[CrossRef\]](#)
- Carlton, A.G.; Wiedinmyer, C.; Kroll, J.H. A review of Secondary Organic Aerosol (SOA) formation from isoprene. *Atmos. Chem. Phys.* **2009**, *9*, 4987–5005. [\[CrossRef\]](#)
- Griffin, R.J.; Cocker III, D.R.; Flagan, R.C.; Seinfeld, J.H. Organic aerosol formation from the oxidation of biogenic hydrocarbons. *J. Geophys. Res. Atmos.* **1999**, *104*, 3555–3567. [\[CrossRef\]](#)
- Kanakidou, M.; Seinfeld, J.H.; Pandis, S.N.; Barnes, I.; Dentener, F.J.; Facchini, M.C.; Van Dingenen, R.; Ervens, B.; Nenes, A.; Nielsen, C.J.; et al. Organic aerosol and global climate modelling: A review. *Atmos. Chem. Phys.* **2005**, *5*, 1053–1123. [\[CrossRef\]](#)
- Pandis, S.N.; Paulson, S.E.; Seinfeld, J.H.; Flagan, R.C. Aerosol formation in the photooxidation of isoprene and β -pinene. *Atmos. Environ.* **1991**, *25*, 997–1008. [\[CrossRef\]](#)
- Butler, T.M.; Taraborrelli, D.; Brühl, C.; Fischer, H.; Harder, H.; Martinez, M.; Williams, J.; Lawrence, M.G.; Lelieveld, J. Improved simulation of isoprene oxidation chemistry with the ECHAM5/MESSy chemistry-climate model: Lessons from the GABRIEL airborne field campaign. *Atmos. Chem. Phys.* **2008**, *8*, 4529–4546. [\[CrossRef\]](#)

23. Karl, T.G.; Christian, T.J.; Yokelson, R.J.; Artaxo, P.; Hao, W.M.; Guenther, A. The Tropical Forest and Fire Emissions Experiment: Method evaluation of volatile organic compound emissions measured by PTR-MS, FTIR, and GC from tropical biomass burning. *Atmos. Chem. Phys.* **2007**, *7*, 5883–5897. [\[CrossRef\]](#)
24. Ouwersloot, H.G.; Vilà-Guerau de Arellano, J.; Van Heerwaarden, C.C.; Ganzeveld, L.N.; Krol, M.C.; Lelieveld, J. On the segregation of chemical species in a clear boundary layer over heterogeneous land surfaces. *Atmos. Chem. Phys.* **2011**, *11*, 10681–10704. [\[CrossRef\]](#)
25. Kaser, L.; Karl, T.; Yuan, B.; Mauldin III, R.; Cantrell, C.; Guenther, A.B.; Patton, E.; Weinheimer, A.J.; Knote, C.; Orlando, J.; et al. Chemistry-turbulence interactions and mesoscale variability influence the cleansing efficiency of the atmosphere. *Geophys. Res. Lett.* **2015**, *42*, 10894–10903. [\[CrossRef\]](#)
26. Koppmann, R.; Kesselmeier, J.; Meixner, F.; Warnke, J.; Bandur, R.; Hoffmann, T.; Aubrun, S.; Leitl, B.; Schatzmann, M.; Dlugi, R.; et al. Emission and chemical transformation of biogenic volatile organic compounds investigations in and above a mixed forest stand (ECHO): An overview. In Proceedings of the Integrated Land Ecosystem–Atmosphere Processes Study (ILEAPS) International Open Science Conference 2003, Helsinki, Finland, 29 September–3 October 2003; pp. 198–201.
27. Dlugi, R.; Berger, M.; Zelger, M.; Hofzumahaus, A.; Siese, M.; Holland, F.; Wisthaler, A.; Grabmer, W.; Hansel, A.; Koppmann, R.; et al. Turbulent exchange and segregation of HO_x radicals and volatile organic compounds above a deciduous forest. *Atmos. Chem. Phys.* **2010**, *10*, 6215–6235. [\[CrossRef\]](#)
28. Dlugi, R.; Berger, M.; Zelger, M.; Hofzumahaus, A.; Rohrer, F.; Holland, F.; Lu, K.; Kramm, G. The balances of mixing ratios and segregation intensity: A case study from the field (ECHO 2003). *Atmos. Chem. Phys.* **2014**, *14*, 10333–10362. [\[CrossRef\]](#)
29. de Arellano, J.V.-G.; Kim, S.-W.; Barth, M.C.; Patton, E.G. Transport and chemical transformations influenced by shallow cumulus over land. *Atmos. Chem. Phys.* **2005**, *5*, 3219–3231. [\[CrossRef\]](#)
30. Kim, S.W.; Barth, M.C.; Trainer, M. Influence of fair-weather cumulus clouds on isoprene chemistry. *J. Geophys. Res. Atmos.* **2012**, *117*, D10302. [\[CrossRef\]](#)
31. Li, Y.; Barth, M.C.; Patton, E.G.; Steiner, A.L. Impact of in-cloud aqueous processes on the chemistry and transport of biogenic volatile organic compounds. *J. Geophys. Res. Atmos.* **2017**, *122*, 11131–11153. [\[CrossRef\]](#)
32. Kim, S.W.; Barth, M.C.; Trainer, M. Impact of turbulent mixing on isoprene chemistry. *Geophys. Res. Lett.* **2016**, *43*, 7701–7708. [\[CrossRef\]](#)
33. Li, Y.; Barth, M.C.; Chen, G.; Patton, E.G.; Kim, S.W.; Wisthaler, A.; Mikoviny, T.; Fried, A.; Clark, R.; Steiner, A.L. Large-eddy simulation of biogenic VOC chemistry during the DISCOVER-AQ 2011 campaign. *J. Geophys. Res. Atmos.* **2016**, *121*, 8083–8105. [\[CrossRef\]](#)
34. Finnigan, J.J.; Shaw, R.H.; Patton, E.G. Turbulence structure above a vegetation canopy. *J. Fluid Mech.* **2009**, *637*, 387–424. [\[CrossRef\]](#)
35. Raupach, M.R.; Finnigan, J.J.; Brunet, Y. Coherent eddies and turbulence in vegetation canopies: The mixing-layer analogy. *Bound. Layer Meteorol.* **1996**, *78*, 351–382. [\[CrossRef\]](#)
36. Gao, W.; Shaw, R.H.; Paw, U.K.T. Observation of organized structure in turbulent flow within and above a forest canopy. *Bound. Layer Meteorol.* **1989**, *47*, 349–377. [\[CrossRef\]](#)
37. Gao, W.; Shaw, R.H.; Paw, U.K.T. Conditional analysis of temperature and humidity microfronts and ejection/sweep motions within and above a deciduous forest. *Bound. Layer Meteorol.* **1992**, *59*, 35–57. [\[CrossRef\]](#)
38. Brunet, Y. Turbulent flow in plant canopies: Historical perspective and overview. *Bound. Layer Meteorol.* **2020**, *177*, 315–364. [\[CrossRef\]](#)
39. Dupont, S.; Patton, E.G. Influence of stability and seasonal canopy changes on micrometeorology within and above an orchard canopy: The CHATS experiment. *Agric. For. Meteorol.* **2012**, *157*, 11–29. [\[CrossRef\]](#)
40. Clifton, O.E.; Patton, E.G.; Wang, S.; Barth, M.; Orlando, J.; Schwantes, R.H. Large eddy simulation for investigating coupled forest canopy and turbulence influences on atmospheric chemistry. *J. Adv. Model. Earth Syst.* **2022**, *14*, e2022MS003078. [\[CrossRef\]](#)
41. Barbaro, E.; de Arellano, J.V.-G.; Krol, M.C.; Holtzlag, A.A.M. Impacts of aerosol shortwave radiation absorption on the dynamics of an idealized convective atmospheric boundary layer. *Bound. Layer Meteorol.* **2013**, *148*, 31–49. [\[CrossRef\]](#)
42. Barbaro, E.; de Arellano, J.V.-G.; Ouwersloot, H.G.; Schröter, J.S.; Donovan, D.P.; Krol, M.C. Aerosols in the convective boundary layer: Shortwave radiation effects on the coupled land-atmosphere system. *J. Geophys. Res. Atmos.* **2014**, *119*, 5845–5863. [\[CrossRef\]](#)
43. Patton, E.G.; Davis, K.J.; Barth, M.C.; Sullivan, P.P. Decaying scalars emitted by a forest canopy: A numerical study. *Bound. Layer Meteorol.* **2001**, *100*, 91–129. [\[CrossRef\]](#)
44. Li, C.W.Y.; Brasseur, G.P.; Schmidt, H.; Mellado, J.P. Error induced by neglecting subgrid chemical segregation due to inefficient turbulent mixing in regional chemical-transport models in urban environments. *Atmos. Chem. Phys.* **2021**, *21*, 483–503. [\[CrossRef\]](#)
45. Molemaker, M.J.; de Arellano, J.V.-G. Control of chemical reactions by convective turbulence in the boundary layer. *J. Atmos. Sci.* **1998**, *55*, 568–579. [\[CrossRef\]](#)
46. Baker, J.; Walker, H.L.; Cai, X. A study of the dispersion and transport of reactive pollutants in and above street canyons—A large eddy simulation. *Atmos. Environ.* **2004**, *38*, 6883–6892. [\[CrossRef\]](#)
47. Auger, L.; Legras, B. Chemical segregation by heterogeneous emissions. *Atmos. Environ.* **2007**, *41*, 2303–2318. [\[CrossRef\]](#)
48. Bright, V.B.; Bloss, W.J.; Cai, X. Urban street canyons: Coupling dynamics, chemistry and within-canyon chemical processing of emissions. *Atmos. Environ.* **2013**, *68*, 127–142. [\[CrossRef\]](#)

49. Zhong, J.; Cai, X.-M.; Bloss, W.J. Modelling the dispersion and transport of reactive pollutants in a deep urban street canyon: Using large-eddy simulation. *Environ. Pollut.* **2015**, *200*, 42–52. [[CrossRef](#)] [[PubMed](#)]
50. Zhong, J.; Cai, X.-M.; Bloss, W.J. Large eddy simulation of reactive pollutants in a deep urban street canyon: Coupling dynamics with O₃-NO_x-VOC chemistry. *Environ. Pollut.* **2017**, *224*, 171–184. [[CrossRef](#)]
51. Wang, Y.; Ma, Y.-F.; Muñoz-Esparza, D.; Li, C.W.Y.; Barth, M.; Wang, T.; Brasseur, G.P. The impact of inhomogeneous emissions and topography on ozone photochemistry in the vicinity of Hong Kong Island. *Atmos. Chem. Phys.* **2021**, *21*, 3531–3553. [[CrossRef](#)]
52. Wang, Y.; Brasseur, G.P.; Wang, T. Segregation of atmospheric oxidants in turbulent urban environments. *Atmosphere* **2022**, *13*, 315. [[CrossRef](#)]
53. Wang, Y.; Ma, Y.F.; Muñoz-Esparza, D.; Dai, J.; Li, C.W.Y.; Lichtig, P.; Tsang, R.C.W.; Liu, C.H.; Wang, T.; Brasseur, G.P. Coupled mesoscale–microscale modeling of air quality in a polluted city using WRF-LES-Chem. *Atmos. Chem. Phys.* **2023**, *23*, 5905–5927. [[CrossRef](#)]
54. Veres, P.R.; Neuman, J.A.; Bertram, T.H.; Assaf, E.; Wolfe, G.M.; Williamson, C.J.; Weinzierl, B.; Tilmes, S.; Thompson, C.R.; Thames, A.B.; et al. Global airborne sampling reveals a previously unobserved dimethyl sulfide oxidation mechanism in the marine atmosphere. *Proc. Natl. Acad. Sci. USA* **2020**, *117*, 4505–4510. [[CrossRef](#)]
55. Boucher, O. Clouds and Aerosols. In *Climate Change 2013: The Physical Science Basis Contribution of Working Group I to the Fifth Assessment Report of the Intergovernmental Panel on Climate Change*; Cambridge Univ Press: Cambridge, UK, 2013; pp. 571–657.
56. Luo, T.; Wang, Z.; Zhang, D.; Chen, B. Marine boundary layer structure as observed by A-train satellites. *Atmos. Chem. Phys.* **2016**, *16*, 5891–5903. [[CrossRef](#)]
57. Narenpitak, P.; Kazil, J.; Yamaguchi, T.; Quinn, P.; Feingold, G. From sugar to flowers: A transition of shallow cumulus organization during ATOMIC. *J. Adv. Model. Earth Syst.* **2021**, *13*, e2021MS002619. [[CrossRef](#)]
58. Stevens, B.; Bony, S.; Brogniez, H.; Hentgen, L.; Hohenegger, C.; Kiemle, C.; L’Ecuyer, T.S.; Naumann, A.K.; Schulz, H.; Siebesma, P.A.; et al. Sugar, gravel, fish and flowers: Mesoscale cloud patterns in the trade winds. *Q. J. R. Meteorol. Soc.* **2020**, *146*, 141–152. [[CrossRef](#)]
59. Vilà-Guerau de Arellano, J.; Van den Dries, K.; Pino, D. On inferring isoprene emission surface flux from atmospheric boundary layer concentration measurements. *Atmos. Chem. Phys.* **2009**, *9*, 3629–3640. [[CrossRef](#)]
60. Kaser, L.; Patton, E.G.; Pfister, G.G.; Weinheimer, A.J.; Montzka, D.D.; Flocke, F.; Thompson, A.M.; Stauffer, R.M.; Halliday, H.S. The effect of entrainment through atmospheric boundary layer growth on observed and modeled surface ozone in the Colorado Front Range. *J. Geophys. Res. Atmos.* **2017**, *122*, 6075–6093. [[CrossRef](#)]
61. Lenschow, D.H.; Gurarie, D.; Patton, E.G. Modeling the diurnal cycle of conserved and reactive species in the convective boundary layer using SOMCRUS. *Geosci. Model Dev.* **2016**, *9*, 979–996. [[CrossRef](#)]
62. Vilà-Guerau De Arellano, J.; Duynkerke, P.G. Influence of chemistry on the flux-gradient relationships for the NO-O₃-NO₂ system. *Bound. Layer Meteorol.* **1992**, *61*, 375–387. [[CrossRef](#)]
63. Hamba, F. A modified K model for chemically reactive species in the planetary boundary layer. *J. Geophys. Res. Atmos.* **1993**, *98*, 5173–5182. [[CrossRef](#)]
64. Cook, A.W.; Riley, J.J. A subgrid model for equilibrium chemistry in turbulent flows. *Phys. Fluids* **1994**, *6*, 2868–2870. [[CrossRef](#)]
65. Cook, A.W.; Riley, J.J. Subgrid-scale modeling for turbulent reacting flows. *Combust. Flame* **1998**, *112*, 593–606. [[CrossRef](#)]
66. Tong, C.; Wyngaard, J.C.; Khanna, S.; Brasseur, J.G. Resolvable-and subgrid-scale measurement in the atmospheric surface layer: Technique and issues. *J. Atmos. Sci.* **1998**, *55*, 3114–3126. [[CrossRef](#)]
67. Tong, C.; Wyngaard, J.C.; Brasseur, J.G. Experimental study of the subgrid-scale stresses in the atmospheric surface layer. *J. Atmos. Sci.* **1999**, *56*, 2277–2292. [[CrossRef](#)]
68. Horst, T.W.; Kleissl, J.; Lenschow, D.H.; Meneveau, C.; Moeng, C.-H.; Parlange, M.B.; Sullivan, P.P.; Weil, J.C. HATS: Field observations to obtain spatially filtered turbulence fields from crosswind arrays of sonic anemometers in the atmospheric surface layer. *J. Atmos. Sci.* **2004**, *61*, 1566–1581. [[CrossRef](#)]
69. Sullivan, P.P.; Horst, T.W.; Lenschow, D.H.; Moeng, C.-H.; Weil, J.C. Structure of subfilter-scale fluxes in the atmospheric surface layer with application to large-eddy simulation modelling. *J. Fluid Mech.* **2003**, *482*, 101–139. [[CrossRef](#)]
70. Patton, E.G.; Horst, T.W.; Sullivan, P.P.; Lenschow, D.H.; Oncley, S.P.; Brown, W.O.; Burns, S.P.; Guenther, A.B.; Held, A.; Karl, T.; et al. The canopy horizontal array turbulence study. *Bull. Amer. Meteor. Soc.* **2011**, *92*, 593–611. [[CrossRef](#)]

Disclaimer/Publisher’s Note: The statements, opinions and data contained in all publications are solely those of the individual author(s) and contributor(s) and not of MDPI and/or the editor(s). MDPI and/or the editor(s) disclaim responsibility for any injury to people or property resulting from any ideas, methods, instructions or products referred to in the content.